

The sensitivity of landfast sea ice to atmospheric forcing in single-column model simulations: a case study at Zhongshan Station, Antarctica

Fengguan Gu¹, Qinghua Yang¹, Frank Kauker^{2,3}, Changwei Liu¹, Guanghua Hao⁴,
Chao-yuan Yang¹, Jiping Liu⁵, Petra Heil⁶, Xuewei Li¹, Bo Han^{1*}

¹ School of Atmospheric Sciences, Sun Yat-sen University, and Southern Marine Science and Engineering Guangdong Laboratory (Zhuhai), Zhuhai 519082, China

² Alfred Wegener Institute, Helmholtz Centre for Polar and Marine Research, Am Handelshafen 12, 27570 Bremerhaven, Germany

³ Ocean Atmosphere Systems, Tewsstseg 4, 20249 Hamburg, Germany

⁴ Key Laboratory of Marine Hazards Forecasting, National Marine Environmental Forecasting Center, Ministry of Natural Resources, Beijing 100081, China

⁵ Department of Atmospheric and Environmental Sciences, State University of New York at Albany, Albany, NY, USA

⁶ Australian Antarctic Division and Australian Antarctic Program Partnership, Private Bag 80, Hobart, Tas 7001, Australia

Correspondence to: Bo Han (hanb5@mail.sysu.edu.cn)

Abstract

Single-column sea ice models are used to focus on the thermodynamic evolution of the ice. Generally, these models are forced by atmospheric reanalysis in the absence of atmospheric *in situ* observations. Here we assess the sea ice thickness (SIT) simulated by a single-column model (ICEPACK) with *in situ* observations obtained off Zhongshan Station for the austral winter of 2016. In the reanalysis, the surface air temperature is about 1 °C lower, the total precipitation is about 2 mm day⁻¹ larger, and the surface wind speed is about 2 m s⁻¹ higher compared to the *in situ* observations, respectively. We designed sensitivity experiments to evaluate the simulation bias in sea ice thickness due to the uncertainty in the individual atmospheric forcing variables. Our results show that the unrealistic precipitation in the reanalysis leads to a bias of 14.5 cm in sea ice thickness and 17.3 cm in snow depth. In addition, our data show that increasing snow depth works to gradually

30 inhibit the growth of sea ice associated with thermal blanketing by the snow due to changing the
31 vertical heat flux. Conversely, given suitable conditions, the sea ice thickness may grow suddenly
32 when the snow load gives rise to flooding and leads to snow-ice formation. Shortcomings of this
33 simulation study are also discussed.

34

35 **1 Introduction**

36 Sea ice plays an essential role in the global climate system by reflecting solar radiation and
37 regulating the heat, moisture, and gas exchanges between the ocean and the atmosphere. In contrast
38 to the rapid decline of sea ice extent and volume in the Arctic (Stroeve et al., 2012; Lindsay and
39 Schweiger, 2015), satellite observations show a slight increase in the yearly-mean area of Antarctic
40 sea ice since the late 1970s (Parkinson and Cavalieri, 2012) followed by a rapid decline from 2014
41 (Parkinson, 2019) and a renewed increase in most recent years (Chemke and Polvani, 2020).
42 Although the sudden decline of Antarctic sea ice is yet to be attributed (Parkinson, 2019), the spatial
43 pattern of Antarctic sea ice changes is suggested to be primarily caused by changes in the
44 atmospheric forcing. For example, the rapid ice retreat in the Weddell Sea from 2015 to 2017 has
45 been associated with the intensification of northerly wind (Turner et al., 2017), while the phase of
46 the southern annular mode (SAM) significantly modulates the sea ice in the Ross Sea and elsewhere,
47 especially in November 2016 (Stuecker et al., 2017; Schlosser et al., 2018; Wang et al., 2019a).

48 Landfast sea ice, the immobile fraction of the sea ice, is mainly located near coastal regions of
49 Antarctica, and its change is assumed to be indicative of the evolution of total Antarctic sea ice (Heil
50 et al., 1996; Heil, 2006; Lei et al., 2010; Yang et al., 2016a). Unlike drifting sea ice, the change in
51 landfast sea ice is dominated by thermodynamic processes, which single-column sea-ice models can
52 well capture (Heil et al., 1996; Lei et al., 2010; Yang et al., 2016b; Zhao et al., 2017; Liu et al.,
53 2022). Furthermore, a single-column sea ice model is a useful tool to evaluate the impacts of
54 different atmospheric forcings on the sea ice evolution because of the relatively simple structure of
55 the physical processes (Cheng et al., 2013; Wang et al., 2019b; Merkouriadi et al., 2020). In this
56 study, a state-of-the-art single-column sea ice model, ICEPACK, is chosen to investigate the
57 sensitivity of landfast sea ice to atmospheric forcing for the region off Zhongshan Station in Prydz
58 Bay, East Antarctica (Figure 1).

59 Due to the lack of *in situ* observation, the majority of sea ice studies, especially for the Antarctic,

60 rely on numerical models. Realistic atmospheric forcing is critical for reliable model simulations.
61 Although being criticized for significant deviations from *in situ* observations (Bromwich et al., 2007;
62 Vancoppenolle et al., 2011; Wang et al., 2016; Barthélemy et al., 2018), atmospheric reanalysis data
63 are assumed to offer reasonable atmospheric forcing for large-scale sea ice models for the Antarctic
64 (Zhang, 2007; Massonnet et al., 2011; Zhang, 2014; Barthélemy et al., 2018). Previous studies
65 reported a large spread between four global atmospheric reanalysis products and *in situ* observations
66 in the Amundsen Sea Embayment (Jones et al., 2016). Moreover, studies showed that directly using
67 atmospheric reanalysis as forcing for models causes significant biases in the Arctic sea ice
68 simulations (Lindsay et al., 2014; Wang et al., 2019b). Similar results, accentuated by the sparseness
69 of atmospheric observations entering the reanalysis, can be foreseen for Antarctica. Therefore, the
70 atmospheric forcing needs to be evaluated carefully before simulating Antarctic sea ice. To our
71 knowledge, few studies have given a quantitative evaluation of the effect of different atmospheric
72 forces on sea ice simulations in Antarctica.

73 The coastal landfast sea ice in Prydz Bay is generally first-year ice. It usually fractures and is
74 exported or melts out completely between December and the following February, and refreeze
75 occurs from late February onwards (Lei et al., 2010). This seasonal cycle is representative of
76 Antarctic landfast sea ice. This study aims to evaluate the contributions of the various atmospheric
77 forcing variables on landfast sea ice growth. The snow cover exerts influence on the evolution of
78 the vertical sea ice-snow column via a number of mechanisms, including the formation of snow-ice
79 added by flooding (Leppäranta, 1983), superimposed ice (Kawamura et al., 1997), and insulating
80 impact (Massom et al., 2001). Understanding the snow depth is a primary concern here.

81 Two sets of atmospheric forcing have been chosen. The first is spatially interpolated ERA5 onto
82 the location of the observation site, and the second is using *in situ* atmospheric observations. It is
83 well-known that the simulation biases of numerical models are introduced through many
84 shortcomings, including unrealistic surface boundary conditions (here: atmospheric forcing),
85 imperfect physical process formulations, computational errors. Understanding the uncertainty in sea
86 ice simulations as well as the sea ice response pattern to atmospheric forcing due to imperfect
87 surface boundaries is a prerequisite for successful simulations and needs to be assessed first.

88 This study is arranged as follows: Section 2 introduces the *in situ* observations, the numerical
89 model, and the reanalysis. The main results are given in section 3, focusing on different kinds of

90 atmospheric forcing on sea ice and snow. Shortcomings, discussions and conclusions follow in
91 sections 4, 5 and 6.

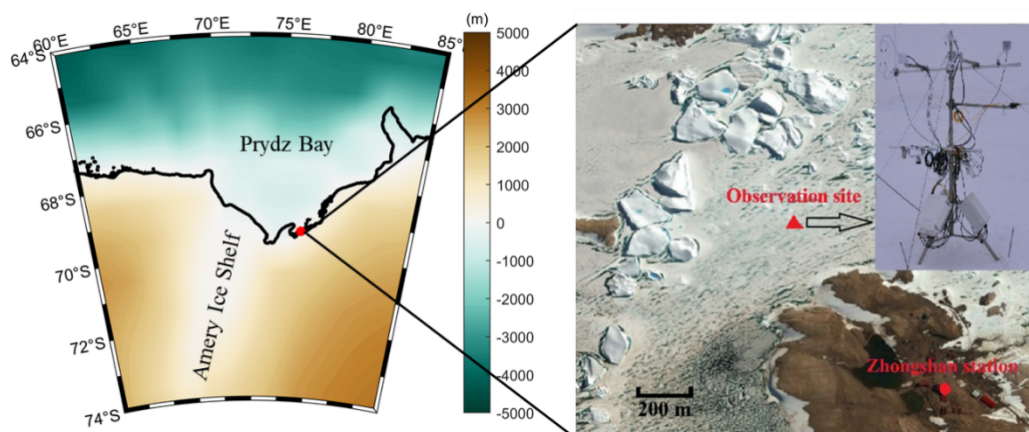
92

93 **2 Materials and methods**

94 **2.1 Meteorological observations**

95 The site of sea ice observation locates in the coastal area off Zhongshan Station
96 [(69°22'S,76°22'E); Figure 1], East Antarctica. The meteorological data were collected at a year-
97 round manned weather observatory run at Zhongshan Station in 2016, which is 1 km inland from
98 the sea ice observation site and 15 m above sea level. Snowfall is measured every 12 hours at the
99 Russian Progress II station (located ~1 km to the southeast of Zhongshan Station). The short- and
100 long-wave radiation fluxes were measured every minute with a net radiometer mounted 1.5 m above
101 the surface on a tripod (Yang et al., 2016a). Other meteorological variables are available as hourly
102 data, including 2 m air temperature (T_{2m}), surface pressure (P_a), specific humidity (calculated from
103 dew-point temperature and P_a), potential temperature (calculated from T_{2m} and P_a), air density
104 (calculated by T_{2m} and P_a) and 10 m wind speed (U_{10}) (Hao et al., 2019; Hao et al., 2020; Liu et al.,
105 2020).

106



107

108 Figure 1 Location of landfast sea ice surface measurements near Zhongshan Station. The solid
109 triangle denotes the observation site, the solid circle marks Zhongshan Station. The color on the left
110 represents the terrain.

111

112

113 **2.2 Sea ice thickness measurement**

114 A thermistor-chain unit developed by Taiyuan University of Technology (TY) was used to
115 measure sea ice thickness in austral winter 2016. This unit is composed of two parts: the control unit
116 and the thermistor chain. The controller initiates data acquisitions and records and stores the
117 temperature measurements. The thermistor chain is 3 m long with 250 equidistant thermistors. Their
118 sensitivity is 0.063 °C, and the measurement accuracy is ± 0.1 °C. The thermistor chain
119 simultaneously records the vertical temperature profile across the near-surface atmosphere, snow
120 cover, sea ice, and surface seawater. The measurement frequency is hourly. Details about the
121 instruments can be found in Hao et al. (2019).

122 Snow thickness close to the thermistor unit is measured weekly using a ruler with an accuracy
123 of ± 0.2 cm. Sea ice thickness is measured with a ruler through a drill hole (5 cm diameter) weekly.
124 The measurement accuracy is ± 0.5 cm. The average thickness obtained from three close-by sites is
125 retained. Sea-surface temperature and sea-surface salinity are measured in the drill holes weekly
126 using a Cond 3210 set 1 (Hao et al., 2019).

127

128 **2.3 Atmospheric reanalysis data**

129 The European Centre for Medium-range Weather Forecasts (ECMWF) released ERA5, the new
130 reanalysis product in 2017, updated in near real-time (Hersbach and Dee, 2016; Hersbach et al.,
131 2020). The complete ERA5 dataset, extending back to 1950, has been available to the end of 2019
132 during this study. Compared with the popular ERA-Interim reanalysis, there are several significant
133 improvements in ERA5, including much higher resolutions (both spatially and temporally). ERA5
134 has global coverage with a horizontal resolution of 31 km by 31 km at the equator and 10 km by 31
135 km at the latitude of Zhongshan Station. The ERA5 resolves the vertical atmosphere profile using
136 137 vertical pressure levels from the surface up to a geopotential height of 0.01 hPa. ERA5 provides
137 hourly analysis and forecast fields and applies a four-dimensional variational data assimilation
138 system (4D-var). ERA5 includes various reprocessed quality-controlled data sets, for example, the
139 reprocessed version of the Ocean and Sea Ice Satellite Application Facilities (OSI SAF) sea ice
140 concentration (Hersbach and Dee, 2016; Hersbach et al., 2020).

141 For comparison and evaluation against the observation in this study, gridded data from ERA5
142 has been bilinearly interpolated to the observation site (detailed in 2.1). Directly using atmospheric

143 forcing from coarse grid cells to interpolate to the observation site, although widely accepted in the
 144 previous studies (e.g., Urraca et al., 2018; Wang et al., 2019b), may cause errors. We have checked
 145 the performance of ERA5 and found that the spatial difference of surface atmospheric variables
 146 around the observation site is relatively small, indicating the choice of interpolation techniques will
 147 not affect the conclusion of this study.

148

149 **2.4 ICEPACK**

150 ICEPACK is a column-physics component of the Los Alamos Sea Ice Model (CICE) V6 and is
 151 maintained by the CICE Consortium. ICEPACK incorporates column-based physical processes that
 152 affect the area and thickness of sea ice. It includes several options for simulating sea ice
 153 thermodynamics, mechanical redistribution (ridging), and associated area and thickness changes. In
 154 addition, the model supports several tracers, including ice thickness, enthalpy, ice age, first-year ice
 155 area, deformed ice area and volume, melt ponds, and biogeochemistry (Hunke et al., 2019).
 156 ICEPACK Version 1.1.1 was used in this study, and detailed options of physical parameterizations
 157 and model settings for the ICEPACK are summarized in Table 1. We employ ICEPACK to distribute
 158 the initial ice thickness to each ice thickness category using a distribution function:

$$159 \quad p_i = \frac{\max(2 \times h \times H_i - H_i^2, 0)}{\sum_i \max(2 \times h \times H_i - H_i^2, 0)}, \quad i = 1 \cdots N, \quad (1)$$

160 Where h is the initial ice thickness, H_i is the prescribed ice thickness category (0–0.6, 0.6–1.4, 1.4–
 161 2.4, 2.4–3.6, and above 3.6 m~; same as for Arctic simulations), N is the number of ice thickness
 162 categories.

163 Table 1 Detailed options of physical parameterizations and model settings for the ICEPACK.

ICEPACK	Value
time step	3600 s
Number of layers in the ice	7
Number of layers in the snow	1
Ice thickness categories	5 (Bitz et al., 2001)
Initial ice thickness	99.5 cm (observed)
Initial snow depth	11.5 cm (observed)
Albedo scheme	CCSM3 (Collins et al., 2006)
Ice thermodynamic	Mushy-layer (Turner et al., 2013)
Shortwave radiation	Delta-Eddington (Briegleb and Light, 2007)
Snowdrift	Not implemented in ICEPACK 1.1.1
Melt ponds (superimposed ice)	Not used in this study
Ocean heat transfer coefficient	0.006 (Maykut and McPhee, 1995)

SST restoring time scale (days)	0 (use observed SST as oceanic forcing)
Ocean friction velocity minimum (m/s)	0.0005 (Tsamados et al., 2013)

164 The atmospheric forcing for the ICEPACK model consists of observations of downward short-
165 and long-wave radiation, 2 m air temperature, specific humidity, total precipitation, potential
166 temperature, 2 m air density, and 10 m wind speed. The oceanic forcing includes sea surface
167 temperature, sea surface salinity, and oceanic mixed layer depth. The period concerned in this study
168 is from April 22, when observed sea ice generally starts to grow, to November 22, 2016. Since there
169 are no observations of the ocean’s mixed-layer depth, we set it to 10 m based on a previously
170 published study (Zhao et al., 2019).

171

172 **3 Results**

173 **3.1 Surface atmospheric conditions near the observation site**

174 First, we compare the eight atmospheric variables used to force ICEPACK (surface downward
175 shortwave radiation (R_{sd}), surface downward long-wave radiation (R_{ld}), surface air temperature (T_a),
176 specific humidity (Q_a), precipitation (P), air potential temperature (θ_a), air density (ρ_a), wind speed
177 (U_a) with the respective *in situ* observation. Table 2 lists the bias (reanalysis minus observation),
178 bias ratio (ratio between the bias and the observation value), the mean value of the *in situ* observation
179 (Mean_Obs), the correlation coefficient (Corr.), and the root-mean-square deviation (RMSD)
180 between the interpolated ERA5 data and the observation. In general, all eight variables from the two
181 sources closely follow each other (Corr. > 0.85), except for P and U_a . In this study, the main attention
182 is on the atmospheric variables T_a , P , and U_a for three reasons: (1) Previous studies have shown that
183 from all atmospheric forcing variables, uncertainties in T_a , P , and U_a exert a significant impact on
184 the sea ice thickness (Cheng et al., 2008). (2) Surface wind may affect the snow cover in two ways:
185 sublimation due to surface turbulent heat flux (Fairall et al., 2003; Gascoïn et al., 2013) and the
186 snowdrift process (Thiery et al., 2012). (3) P and U_a from the reanalysis have the largest bias ratio
187 compared to the *in situ* observations.

188 The timing of daily variations of T_a is well represented by ERA5, especially for strong cooling
189 events (Figure 2a). However, ERA5 tends to underestimate warm events by a few degrees as well
190 as cold events where differences exceeding 10 °C may occur (Figure 2d). During the entire
191 observation period in 2016, T_a from ERA5 was 1.2 °C lower than the *in situ* observation. Also,

192 previous studies reported similar disagreement in T_a between observation and reanalysis in
 193 Antarctica (Bracegirdle and Marshall, 2012; Fréville et al., 2014). The cold bias of T_a in the
 194 reanalysis was suggested to be caused by the ice surface schemes that cannot accurately describe
 195 the ice-atmosphere interactions of strongly stable stratified boundary layers that are frequent in
 196 Antarctica.

197

198 Table 2 Comparison of atmospheric forcing between ERA5 reanalysis and *in situ* observations.

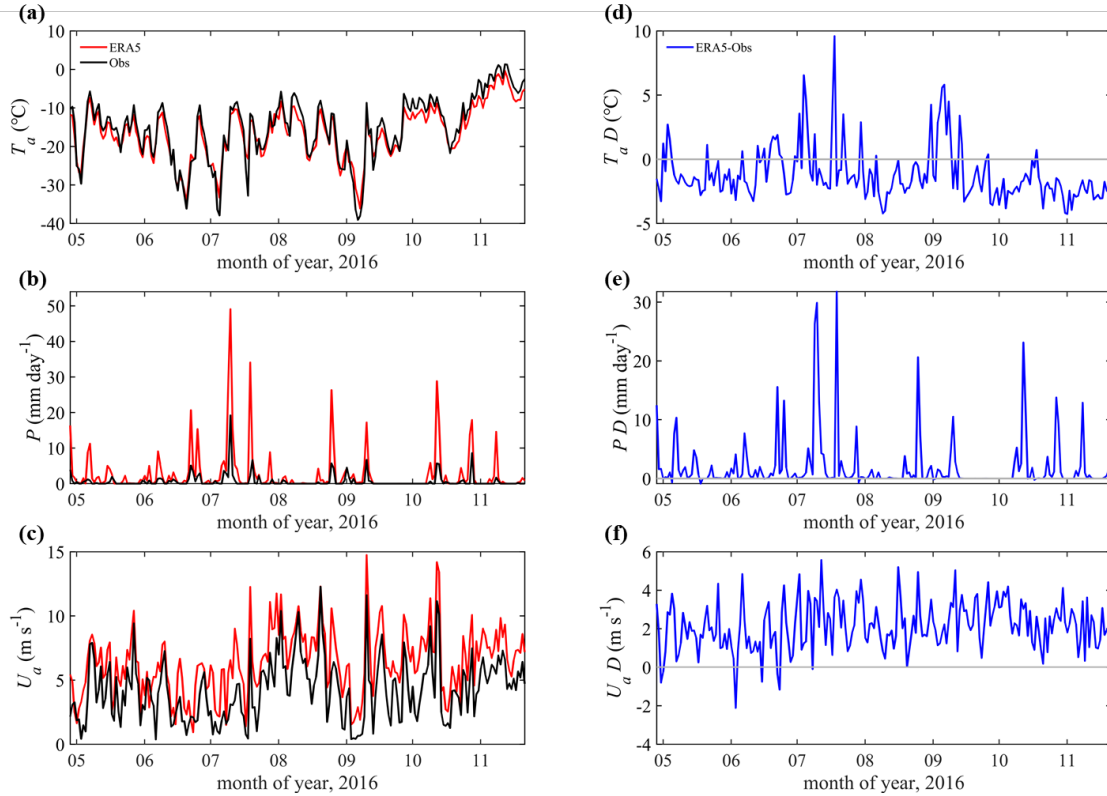
Variable	Bias	Bias ratio (%)	Mean_Obs	Corr	RMSD
R_{sd} ($W\ m^{-2}$)	6.115	9.031	67.714	0.967	40.981
R_{ld} ($W\ m^{-2}$)	-19.153	-9.672	198.023	0.869	28.753
T_a (K)	-1.168	-0.453	257.809	0.967	2.820
Q_a ($10^{-4}\ kg\ kg^{-1}$)	-0.769	-9.326	8.247	0.950	1.987
P ($mm\ day^{-1}$)	2.010	303.509	0.660	0.639	0.825
Θ_a (K)	0.290	0.112	259.437	0.965	2.609
ρ_a ($kg\ m^{-3}$)	-0.021	-1.592	1.322	0.958	0.026
U_a ($m\ s^{-1}$)	2.145	50.735	4.228	0.765	2.989

199

200 The reanalyzed variable with the largest bias ratio from the observation is precipitation (Figure
 201 2b). Hourly precipitation from ERA5 was accumulated into daily data and compared with the
 202 nearest available daily precipitation records from the Progress II station. The maximum daily mean
 203 precipitation can reach $19.1\ mm\ day^{-1}$ (July 11, 2016), with an average of $0.66\ mm\ day^{-1}$ from April
 204 29 to November 22, 2016. While ERA5 captures the main precipitation events, it significantly
 205 overestimated the magnitude of precipitation events, especially in July. In this month, the mean
 206 precipitation rate from ERA5 is $5.83\ mm\ day^{-1}$, while the observed is only $1.42\ mm\ day^{-1}$. From
 207 April to November, the accumulated precipitation from ERA5 is about 300% larger than that in the
 208 *in situ* observations. Nevertheless, using precipitation from Progress II for Zhongshan Station may
 209 be questioned because of the distance of about 1 km to Zhongshan Station. Moreover, the snowdrift
 210 due to strong surface wind can affect the precipitation observation and the local accumulated snow
 211 mass, which may further cause a significant bias in snow depth between simulation and observation.

212

213



214

215 Figure 2 Time series of daily (a) surface air temperature, (b) precipitation rate, and (c) wind speed
 216 (10 m above the surface). The ERA5 reanalysis data are indicated as red lines. Observations are
 217 marked by black lines. (d-f) show the difference (marked by 'D') between ERA5 and the observation
 218 (ERA5-observation). The differences are marked by blue lines. The gray lines denote the zero line.

219

220 The observed U_a varied from 0.01 m s^{-1} to 12.3 m s^{-1} with an average of 4.2 m s^{-1} (Figure 2c).
 221 ERA5 well captured the daily and seasonal variation of U_a , but an overestimation of 2.1 m s^{-1} should
 222 be noted, mainly when observed $U_a > 5 \text{ m s}^{-1}$. One explanation for such overestimation is that the
 223 numerical model underlying ERA5 cannot represent the surface roughness and the katabatic wind
 224 in a region with complex orography (Tetzner et al., 2019; Vignon et al., 2019).

225

226 3.2 Simulation forced by observed *in situ* atmospheric variables

227 The simulation bias of sea ice thickness and snow depth is impacted by many aspects, including
 228 unrealistic atmospheric and oceanic forcing and shortcomings in the applied numerical model. In
 229 this study, we mainly focus on the influence of imperfect atmospheric forcing.

230 The sea ice thickness (Obs) measured through a hole drilled is increasing from April 29 (100 ± 2

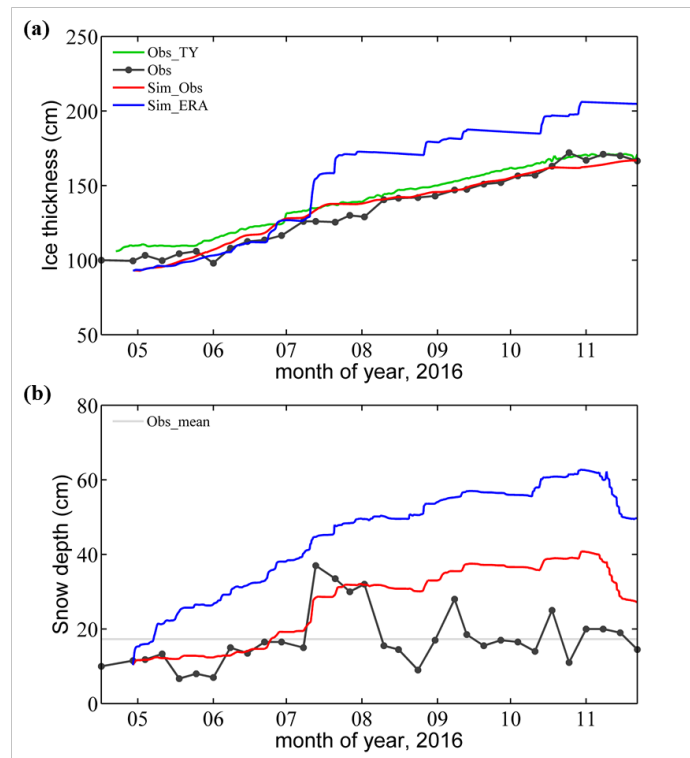
231 cm) to October 25 (172 ± 2 cm), remaining level from there on (Figure 3a). The ice thickness deduced
232 from the TY (Obs_TY) thermistor-chain buoy shows a similar result: sea ice thickness increased
233 from 106 cm on April 22 to 171 cm on November 17. In November, the sea ice thickness (Obs and
234 Obs_TY) is stationary, indicating a thermodynamic equilibrium between heat loss to the atmosphere
235 and heat gain from the ocean (Yang et al., 2016a; Hao et al., 2019).

236 When forced by atmospheric *in situ* observations (Sim_Obs), the simulated sea ice thickness
237 agrees well with the observed thickness with a mean bias of less than 1 cm over the growing season.
238 We attribute the excellent simulation result to the fact that the seasonal evolution of landfast is driven
239 mainly by thermal processes, which ICEPACK captures well.

240 The average snow depth from observation is 17 cm during the ice-growth season, with low snow
241 depth measured before July 11 (Figure 3b). After that, the snow depth increases rapidly up to about
242 37 cm, associated with a precipitation event arising from a single synoptic system. Then it decreases
243 below the seasonal mean (Obs_mean), followed by two secondary maxima (> 25 cm) on September
244 8 and October 18, respectively.

245 The snow depth in Sim_Obs tracks the observation closely before August 2 (Figure 3b). Then,
246 the Observed snow depth decreased quickly from about 30 cm to about 10 cm, while the Sim_Obs
247 snow depth continued to increase gradually until the onset of surface melting in November. We
248 attribute the Observed quick decrease of snow depth to the effect of the snowdrift because the
249 surface wind stayed above 5 m s^{-1} for most of August (Figure 2c), giving rise to snowdrift, a process
250 not implemented in the version of ICEPACK used here. The snowdrift might cause a significant
251 spatial difference in accumulated snow patterns (Liston et al., 2018), which may be responsible for
252 the large deviation in snow depth between Sim_Obs and Observation. In addition, Sim_Obs
253 underestimated the snow depth on July 11. As discussed above, using nonlocal observed
254 precipitation from Progress II should be questioned.

255 Using observed meteorological variables as atmospheric forcing in ICEPACK produced
256 unreliable snow depth while the sea ice thickness was in reasonably good agreement. In other words,
257 the enormous bias in snow depth seems to have little effect on the sea ice thickness in the simulation.
258 This counter-intuitive finding is of great interest to us because it disobeys the general realization
259 that the snow layer significantly modifies the energy exchange on top of the sea ice. Potential causes
260 for this result will be discussed later.



262

263 Figure 3 Time series of (a) sea ice thickness and (b) snow depth during the freezing season. Black
 264 solid lines with black points show the observations from the drill hole (Obs). Green solid lines show
 265 the ice thickness derived from the TY buoy (Obs_TY). Red solid lines show the simulation results
 266 under *in situ* atmospheric forcing (Sim_Obs), and blue solid lines are simulation results under ERA5
 267 forcing (Sim_ERA). In (b), the gray solid line shows the seasonal mean snow depth observation
 268 (Obs_mean).

269

270 3.3 Simulation forced by ERA5 atmospheric variables

271 When forced by ERA5 (Sim_ERA), the simulated sea ice thickness shows significant deviations
 272 from observation (Figure 3a). The deviation is only about 1 cm before July 11, when a heavy
 273 precipitation event ($\sim 19 \text{ mm day}^{-1}$) happened. After the precipitation episode, the offset in the sea
 274 ice thickness between Sim_ERA and observation was almost constant, about 33 cm.

275 In contrast to sea ice thickness, the precipitation from ERA5 causes an overestimation in snow
 276 depth for the entire simulation period. The snow depth from Sim_ERA is much greater than
 277 observation, even before July 11 (Figure 3b). During the heavy precipitation event (Figure 2b), the
 278 observed snow depth increased from 20 cm to about 40 cm. Although the precipitation rate from

279 ERA5 ($\sim 40 \text{ mm day}^{-1}$) is two times larger than the observation, it caused little response in the
 280 simulated snow depth. The snow depth increase is near-linear, from about 10 cm to almost 60 cm.
 281

282 3.4 Sensitivity analysis

283 To determine which atmospheric variables, including T_a , P , and U_a , are the most crucial in the
 284 sea ice simulation, we designed a set of sensitivity simulation experiments named SEN1. The
 285 simulation under the forcing from the *in situ* observed atmospheric variables is the control
 286 experiment and is named Sim_Obs. In each experiment of SEN1, one atmospheric variable is
 287 replaced by the corresponding variable from ERA5, while all others are identical to those of the
 288 control experiment. In Table 3, the averaged bias between the simulation and the observation of the
 289 outputs (ice thickness and snow depth) and the bias ratio of forcing atmospheric variables are listed
 290 separately.

291

292 Table 3 Bias of ice thickness, snow depth, and bias ratio for each forcing variable come from Table
 293 2. ‘All’ means using the full set of ERA5 atmospheric forcing.

Variable	Bias		Bias ratio (%)
	Ice (cm)	Snow (cm)	Forcing
R_{sd} (W m^{-2})	-0.044	-0.130	9.031
R_{ld} (W m^{-2})	3.050	2.243	-9.672
T_a (K)	0.001	0.029	-0.453
Q_a ($10^{-4} \text{ kg kg}^{-1}$)	1.099	-1.299	-9.326
P (mm day^{-1})	14.519	17.312	303.509
Θ_a (K)	-0.483	0.407	0.112
ρ_a (kg m^{-3})	0.119	-0.071	-1.592
U_a (m s^{-1})	-0.311	-3.421	50.735
<i>All</i>	16.824	17.882	/

294

295 To determine the sensitivity of sea ice and snow depth near Zhongshan station on atmospheric
 296 forcing, we designed a set of numerical experiments named SEN2. In the control run, the forcing of
 297 the simulation directly used the means of observed atmospheric variables (Mean_Obs in Table 4).
 298 For a specific atmospheric variable, we build a set of sensitive runs. The focused atmospheric
 299 variable changed from its mean (Range in Table 4), and other variables are the same as the control

300 run. Considering the actual range of each observed variable on an interannual scale (Van Den Broeke
 301 et al., 2004; Jakobs et al., 2020; Roussel et al., 2020), we set the maximum change in T_a , Θ_a , and ρ_a
 302 to 2%, and other atmospheric variables to 50%. Then, we concluded the sensitivity of sea ice and
 303 snow to each atmospheric forcing from its corresponding sensitive runs. Because sea ice and snow
 304 depth show a quasi-linear response to the change in each specific atmospheric forcing (not shown),
 305 the choice of the variable's range will not alter the sensitivity results.

306

307 Table 4 The atmospheric forcing (Mean_obs for the control run and range for the sensitive run), and
 308 sensitivity from SEN2.

Variable	Mean_Obs (Control)	Range (%)	Sensitivity	
			Ice (cm/%)	Snow (cm/%)
R_{sd} ($W\ m^{-2}$)	67.714	± 50	-0.033	-0.008
R_{ld} ($W\ m^{-2}$)	198.023	± 50	-0.368	-0.201
T_a (K)	257.809	± 2	-1.247	-0.526
Q_a ($10^{-4}\ kg\ kg^{-1}$)	8.247	± 50	-0.025	0.029
P ($mm\ day^{-1}$)	0.660	± 50	-0.032	0.135
Θ_a (K)	259.437	± 2	-1.297	-0.491
ρ_a ($kg\ m^{-3}$)	1.322	± 2	-0.054	0.021
U_a ($m\ s^{-1}$)	4.228	± 50	-0.054	-0.022

309

310 Comparing the individual biases in Table 3, it turns out that P and R_{ld} from ERA5 contribute to
 311 the bias in sea ice thickness most strongly. For snow depth, P , U_a , and R_{ld} contribute the largest. In
 312 Table 4, the sensitivity of ice thickness and snow depth to each atmospheric variable are listed.
 313 Comparing the individual sensitivity, it turns out that the sea ice thickness and snow depth are most
 314 sensitive to T_a and Θ_a . However, T_a from ERA5 is close to the *in situ* observation, so the simulated
 315 sea ice thickness and snow depth are hardly impacted (Table 3). The results from SEN1 reveal that
 316 the overestimation in P in ERA5 is the primary source of the overestimation of sea ice thickness
 317 and snow depth, even with less sensitivity to precipitation (Table 4).

318 To clarify the effect of specific forcing further, we replaced the x forcing in Sim_Obs with the
 319 corresponding ERA5 variable and named it Sim_ERA_x. Compared with Sim_Obs, Sim_ERA_P
 320 overestimates the snow depth since May (Figure 4b) and shows a significant positive bias in sea ice
 321 thickness after July 11 (Figure 4a). Before July 11, the sea ice thickness from Sim_ERA_P was even

322 smaller than that from Sim_Obs.

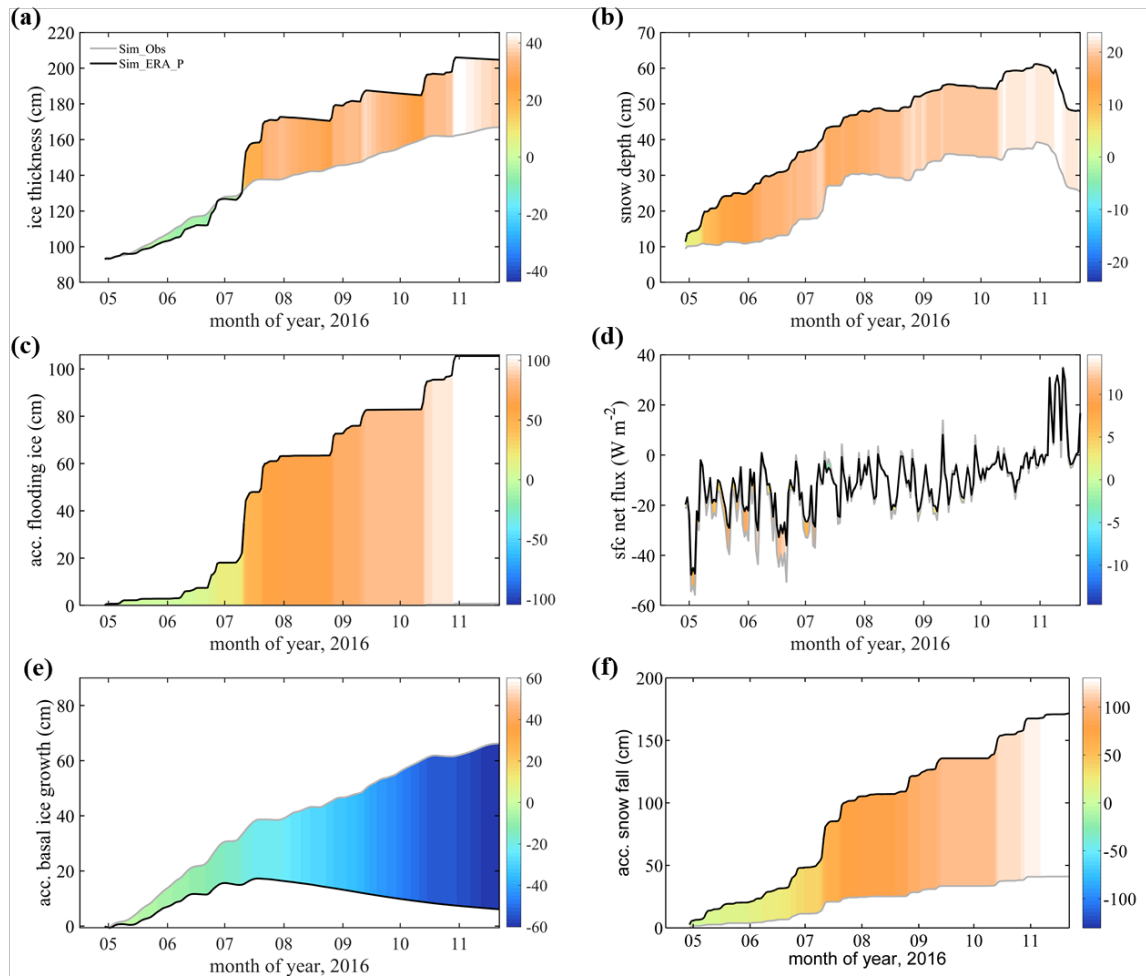
323 To find out why the snow and sea ice behaves differently, we first investigate the net heat flux
324 into the snow surface H_N (positive downward):

$$325 \quad H_N = Rn + Hs + Hl, (2)$$

326 where Rn , Hs , and Hl are the net surface radiation flux, the sensible heat flux, and the latent heat
327 flux, respectively. All energy fluxes are defined as positive downward. Because the simulated snow
328 layer in SIM_ERA_P is much deeper than in SIM_Obs, the difference in H_N reflects the modification
329 of the surface energy flux due to the changed snow layer. From Figure 4d, it can be deduced that the
330 overestimation of snow depth in SIM_ERA_P results in a positive anomaly of H_N before July 11,
331 which hampers the sea ice growth. Later the difference in H_N becomes relatively small. The
332 dependence of H_N on the snow depth is significant when the snow layer is shallow (<20 cm in this
333 study). If the snow layer is deep enough, its impact on the net surface heat flux ceases.

334 After July 11, the difference in sea ice thickness between the two simulations increases quickly
335 from ~0 to >40 cm (Figure 4a). We attribute that to flooding with subsequent snow-ice formation
336 (Powell and others, 2005). The continuously deepening snow layer reduces the sea ice freeboard.
337 When heavy snowfall occurs, which frequently happens after July 11, the snow load pushes the sea
338 ice surface below sea level, and seawater floods onto the sea ice surface, causing the overlying snow
339 to freeze. This snow-ice formation process will form flooding ice (snow-ice thickness) at the sea ice
340 surface and rapidly increase the total sea ice thickness (Figure 4a). The difference (~100 cm) in
341 accumulated flooding ice (Figure 4c) between Sim_Obs (0.8 cm) and Sim_ERA_P (105.5 cm) is
342 much greater than the difference (~40 cm) in simulated sea ice thickness (Figure 4a), while the net
343 surface heat flux compares well after July 11 (Figure 4d). This difference may be because as the
344 snow-ice process occurs, the increase in sea ice thickness will reduce the heat loss from the ice cover
345 and inhibit the basal growth of sea ice in winter (Figure 4e). The flooding-induced snow-ice
346 formation happens at a rate larger than 0.5 cm per hour after July 11. The snowfall (Figure 2b) is
347 converted to new snow depth at the top surface (Figure 4f) using a snow density of 330 kg m⁻³ in
348 ICEPACK (Hunke et al., 2019). Comparing Figure 4b with Figure 4f, we find that the change in
349 actual snow depth (11 cm) is much lower than the expected accumulated snowfall (57 cm),
350 indicating that the flooding process reduces about four-fifths of snow depth over sea ice.

351



352

353 Figure 4 Times series of (a) sea ice thickness, (b) snow depth, (c) accumulated flooding ice, (d) net
 354 surface heat flux, (e) accumulated basal ice growth, and (f) accumulated snowfall. The gray line
 355 represents the simulation using precipitation from observation (Sim_Obs). The black line represents
 356 the simulation using precipitation from ERA5 (Sim_ERA_P). The color bar represents their
 357 difference (Sim_ERA_P – Sim_Obs).

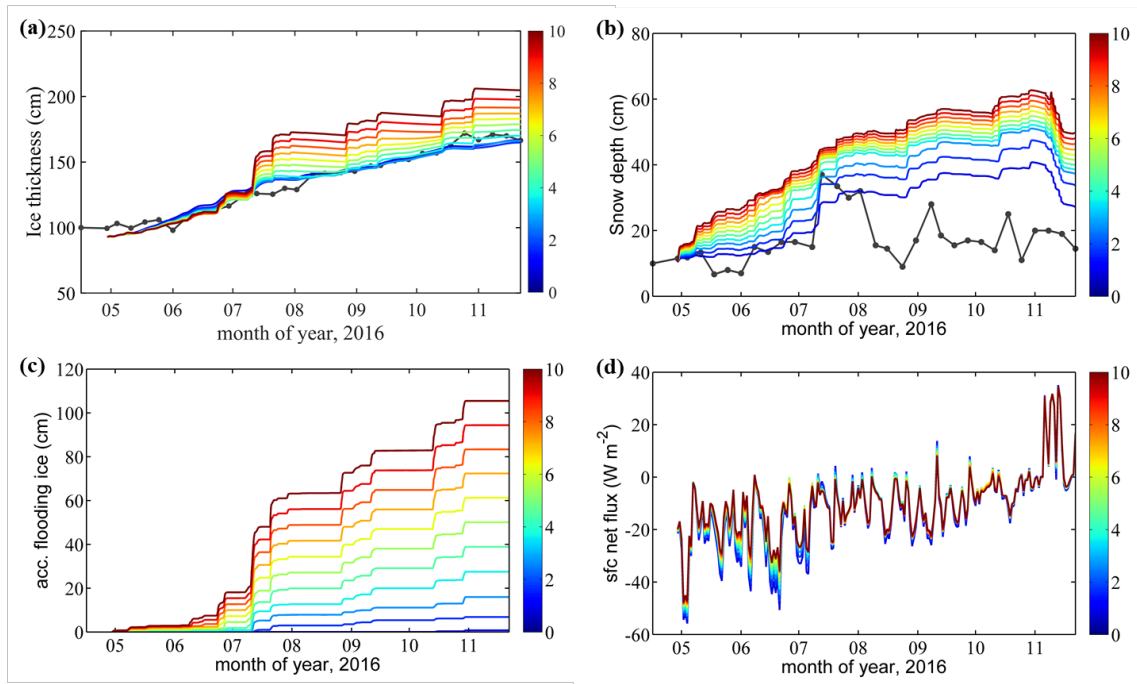
358

3.5 Additional sensitivity simulations on the precipitation bias

359

The precipitation from ERA5 shows the most significant deviation compared to the *in situ*
 360 observation and contributes the largest to the sea ice and snow simulation bias. To determine the
 361 cause of differences in the sea ice and snow response to precipitation, we set up ten sensitivity
 362 experiments named SEN3 (Figure 5). In the n -th experiment, $n \times 10\%$ of the daily difference between
 363 P from ERA5 and the *in situ* observation is added to the observed P on that day. This procedure
 364 gradually increases the magnitude of the precipitation in the experiments while the timing of the
 365 daily precipitation events remains almost unchanged.

366

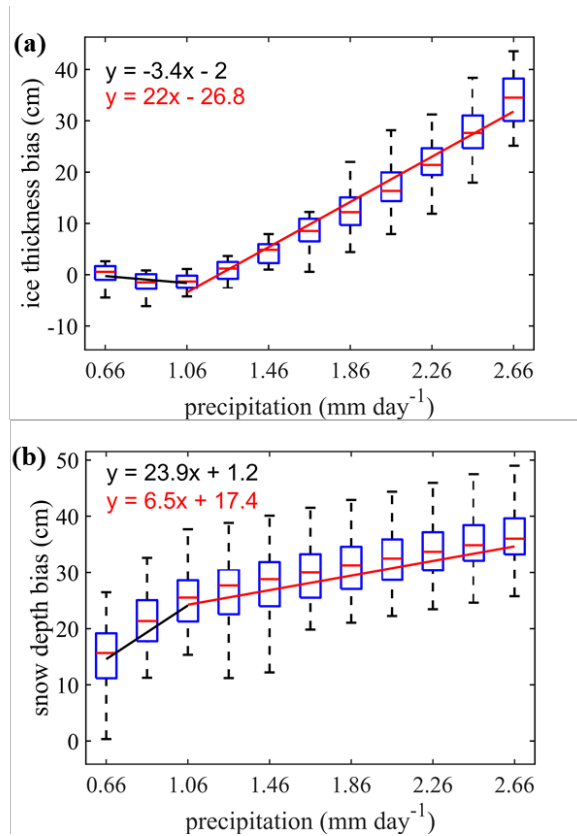


367

368 Figure 5 Time series of the simulated (a) sea ice thickness, (b) snow depth, (c) accumulated flooding
 369 ice, and (d) net surface heat flux in the n experiments of SEN3. The black solid point lines show the
 370 *in situ* observations (Obs). The 11 colored lines denote the 11 sensitivity experiments. When $n = 0$,
 371 precipitation is from the *in situ* observation. When $n = 10$, precipitation is from ERA5.

372

373



374

375 Figure 6 Box plot of simulation bias (simulation minus observation) of (a) sea ice thickness and (b)
 376 snow depth over the daily mean precipitation in the different sensitivity experiments (n increases
 377 from left to right). On the x-axis, 0.66 mm refers to the experiment with n=0 (*in situ* precipitation),
 378 and 2.66 mm refers to the n=10 experiment (ERA5 precipitation). Two linear regression lines (black
 379 and red) are derived for $x \leq 1.06$ mm and $x > 1.06$ mm based on the mean of ice thickness and
 380 snow depth.

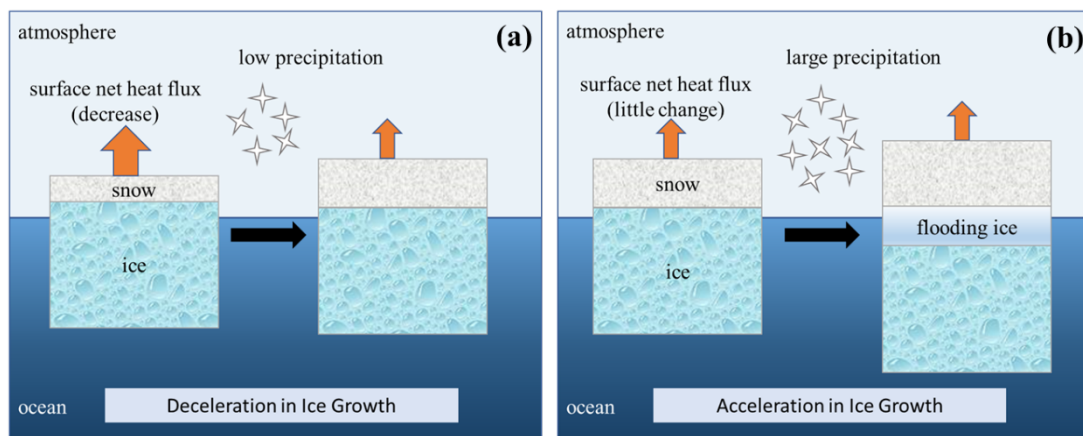
381 We define the bias as the difference between simulations and observations from July 27 to the
 382 end of November. Different start or end dates of this period do not change this result. The bias of
 383 both sea ice thickness and snow depth linearly grows with increasing precipitation (Figure 6). The
 384 simulation bias of the sea ice thickness is relatively small before the precipitation increases by about
 385 1 mm per day. We suggested that the snow-ice formation is small (Figure 5c), and the insulation of
 386 the snow layer (Figure 5d) hampers the sea ice growth. In fact, the simulated sea ice thickness even
 387 decreases (at a rate of $-3.4 \text{ cm}/(\text{mm day}^{-1})$) when the added precipitation is $< 1 \text{ mm day}^{-1}$. When the
 388 added precipitation is $> 1 \text{ mm day}^{-1}$, the simulated sea ice thickness quickly increases at a rate of 22
 389 $\text{cm}/(\text{mm day}^{-1})$.

390 In contrast, the simulated snow depth increases rapidly at $23.9 \text{ cm}/(\text{mm day}^{-1})$ when the enforced

391 precipitation remains small but at a rate of 6.5 cm when the added precipitation is large. This is
 392 because more snow is converted into flooding ice, and the snow-ice formation process strongly
 393 overrules the larger insulation effect from the snow layer, promoting sea ice growth.

394 The snow-ice process is based on Archimedes' Principle. Therefore, the threshold value (1
 395 mm/day⁻¹) is related to the density value of ice, snow, and water in model parameterization as well
 396 as the sea ice thickness and snow depth. If sea ice and snow density, initial snow depth decrease, or
 397 seawater density and initial ice thickness increase, the threshold will increase, and vice versa. These
 398 different effects of increases in precipitation on the snow and sea ice growth are illustrated in Figure
 399 7, emphasizing the role of flooding via snow-ice formation. When the snow layer is shallow,
 400 increases in precipitation will quickly deepen the snow layer and inhibit the growth of sea ice
 401 thickness due to the insulation of snow. The decrease in the surface net heat flux is the dominant
 402 factor. While the snow layer is deep and large precipitation is present, the flooding process induces
 403 snow-ice formation, and the sea ice grows quickly while the snow depth increases only slowly.

404



405

406 Figure 7 Schematic diagram for (a) low precipitation and (b) large precipitation events illustrating
 407 the precipitation effect on sea ice growth. The orange arrows represent surface net heat flux, and
 408 different colored boxes indicate the layer of snow, flooding ice, and sea ice.

409

410 **4 Shortcomings**

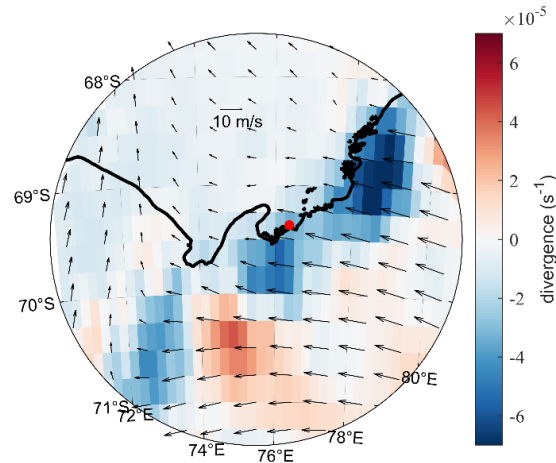
411 The simulated ice thickness and snow depth deviate from the observations in this study (Figure
 412 3). We list the shortcomings that could affect the simulation: 1) Superimposed ice is not considered
 413 in this study; 2) The snow-ice formation might be overestimated on the landfast sea ice in ICEPACK;
 414 3) The snowdrift process has not been involved in the version of ICEPACK used here.

415 Superimposed ice is present in early autumn when the snow starts to melt (Kawamura et al.,
416 1997) and contributes significantly to sea ice growth (up to 20% of mass) (Granskog et al., 2004).
417 Superimposed ice usually corresponds to liquid precipitation or melted snow that permeates
418 downward to form a fresh slush layer and refreezes. The superimposed ice is implemented in
419 ICEPACK via the melt ponds parametrization but has not been considered in this study. Therefore,
420 the simulation may underestimate sea ice thickness and overestimate snow depth compared to the
421 observation in November (Figure 3a). We will apply the melt ponds scheme in the follow-up
422 research work.

423 Flooding-induced snow-ice formation is common in the Antarctic ocean because of the thin ice
424 and heavy snowfall (Kawamura et al., 1997). It can contribute to considerable ice mass (12%-36%)
425 and reduce the snow depth by up to 42-70%, depending on the season and location (Jeffries et al.,
426 2001). The parameterization of the flooding process in the ICEPACK is based on Archimedes'
427 Principle for the pack ice, which might be problematic for the coastal landfast sea ice. With a much
428 larger volume and shallower seawater around than the pack sea ice, part of the coastal landfast sea
429 ice might contact the sea bed rather than float in the sea. Thus, the flooding should be much weaker
430 even with weighted snow cover. Besides, the change in density of ice due to the flooding process is
431 significant (Saloranta, 2000) but not well considered in ICEPACK. For example, a slushy layer of
432 10 cm depth would refreeze within three days from observation (Provost et al., 2017), while the
433 process only needs one day in ICEPACK. Hence, the landfast sea ice growth due to snow-ice
434 formation needs improvement in ICEPACK, especially when the input precipitation is significantly
435 exaggerated, e.g., the ERA5 forcing.

436 Surface drifting snow particles play an essential role in the surface mass balance (Van den
437 Broeke et al., 2004). Figure 3b shows that the observed snow depth has quickly decreased from 32
438 cm on August 2 to 15.5cm on August 10, which should be attributed to the snowdrift because the
439 surface wind is $> 8 \text{ m s}^{-1}$ in most of this period (Figure 2c). Friction velocity becomes sufficiently
440 high to overcome the gravity and bonds between snow particles in this strong wind and raise the
441 snow particles from the surface (van den Broeke et al., 2006; Thiery et al., 2012; Tanji et al., 2021).
442 However, the mean surface wind in ERA5 is convergent around the observation site during the
443 intense wind period (Figure 8), which might not be expected for snow depth to decrease due to
444 snowdrift. The coarse resolution of the atmospheric reanalysis might not produce a realistic surface

445 wind field, which is primarily determined by the local topography (Van Den Broeke et al., 1999;
446 Frezzotti et al., 2005). In addition, surface sublimation of drifting snow particles, which is most
447 significant in warm, dry, and windy weather (Thiery et al., 2012), plays an important role in surface
448 mass balance (Van den Broeke et al., 2004) but has not been involved in ICEPACK yet.



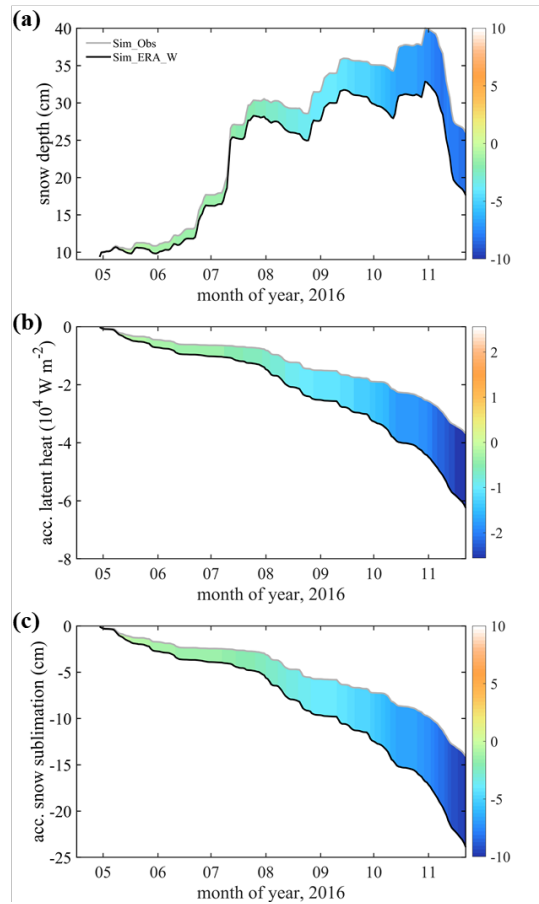
449
450 Figure 8 The mean ERA5 surface wind and divergence from August 2 to 10. The black line
451 represents the coastline, and the red point represents the observation site.

452

453 5 Discussions

454 The surface wind can affect the snow depth by changing the surface heat fluxes (Fairall et al.,
455 2003). Compared with Sim_Obs, Sim_ERA_W gives a $-2.5 \times 10^4 \text{ W m}^{-2}$ lower latent heat flux
456 (positive downward) on average (Figure 9b), i.e., a larger sublimation (Figure 9c), and a reduction
457 of about -3.4 cm of the snow depth (Figure 9a). Therefore, the overestimation in the surface wind
458 from ERA5 partly neutralizes the effect of overestimated precipitation.

459



460

461 Figure 9 Times series of (a) snow depth, (b) accumulated latent heat flux, and (c) accumulated snow
 462 sublimation. The gray line represents the simulation using wind from the observation (Sim_Obs).
 463 The black line represents the simulation using wind from ERA5 (Sim_ERA_W). The color bar
 464 represents their difference (Sim_ERA_W – Sim_Obs).

465 The oceanic forcing also plays an essential role in sea ice evolution (Uotila et al., 2019). Heat
 466 flux from the ocean boundary layer changes the sea ice energy balance (Maykut and Untersteiner,
 467 1971). The ocean heat flux is mainly impacted by summer insolation through open leads, thin ice,
 468 melt ponds (Perovich and Maykut, 1990), and upward heat transfer through vertical turbulent
 469 mixing (McPhee et al., 1999). Because the oceanic observations under sea ice are challenging, most
 470 sea ice models directly use some empirical values, like the default value in CCSM3, to build the
 471 ocean boundary condition (e.g., Yang et al., 2016b; Turner and Hunke, 2015). Although some
 472 oceanic variables, like the water temperature and salinity, are from observation, others refer to
 473 previous studies, like the mixed layer depth. The uncertainty in oceanic forcing might be as
 474 important as the atmospheric ones, which will be focused on in our coming work.

475

476 **6 Conclusions**

477 This work uses the single-column sea ice model ICEPACK forced by the ERA5 atmospheric
478 reanalysis and atmospheric *in situ* observations to simulate snow depth and sea ice thickness at
479 Zhongshan Station, Antarctic. We find that forced by atmospheric variables from *in situ* observations.
480 The ICEPACK can reasonably simulate the sea ice thickness evolution but significantly
481 overestimates the snow depth after the heavy snowfall on July 11. When using atmospheric forcing
482 from ERA5, sea ice thickness simulation is close to observation before July 11 but suddenly
483 increases after the snowfall event.

484 From the sensitivity experiments, we find that the significant deviation in the precipitation of
485 ERA5 contribute to the largest bias in both sea ice thickness and snow depth even though the
486 precipitation is moderately sensitive to sea ice thickness (-0.032 cm/%) and snow depth (0.135
487 cm/%). On average, about 2 mm day⁻¹ more precipitation in ERA5 is found during the observation
488 period, which produces about 14.5 cm excess in sea ice thickness and 17.3 cm more snow depth.

489 We further explore the physical mechanism of the effect of precipitation on ice thickness. Snow-
490 ice formation can be triggered by a heavy snowfall episode, like on July 11. It efficiently produces
491 ice at the sea ice surface, decelerates the snow accumulation, and inhibits sea ice's basal growth.
492 When the snowfall is weak, the snow layer thickens quickly and hampers the sea ice growth through
493 its insulation effect. When the snowfall increases to a certain degree (~1 mm day⁻¹), it will trigger a
494 continuous flooding process, accelerating the sea ice growth and slowing down the snow layer
495 thickening.

496

497 **Acknowledgments**

498 The authors would like to thank ECMWF for the ERA5 reanalysis data set and the Russian
499 meteorological station Progress II for the precipitation observations. We are grateful to CICE
500 Consortium for sharing ICEPACK and its documentation ([https://github.com/CICE-
501 Consortium/Icepack](https://github.com/CICE-Consortium/Icepack)). This study is supported by the National Natural Science Foundation of China
502 (No. 41941009, 41922044), the Guangdong Basic and Applied Basic Research Foundation (No.
503 2020B1515020025), the Southern Marine Science and Engineering Guangdong Laboratory (Zhuhai)
504 (No. SML2020SP007), and CAS "Light of West China" Program (No. E129030101, Y929641001).
505 PH was supported by AAS grant 4506.

506 **References**

507 Barthélemy, A., Goosse, H., Fichefet, T., and Lecomte, O.: On the sensitivity of Antarctic sea ice model
508 biases to atmospheric forcing uncertainties, *Clim. Dynam.*, 51, 1585-1603, 2018.

509 Bitz, C. M., Holland, M. M., Weaver, A. J., and Eby, M.: Simulating the ice - thickness distribution in a
510 coupled climate model, *Journal of Geophysical Research: Oceans*, 106, 2441-2463, 2001.

511 Bracegirdle, T. J., and Marshall, G. J.: The reliability of Antarctic tropospheric pressure and temperature
512 in the latest global reanalyses, *J. Climate*, 25, 7138-7146, 2012.

513 Briegleb, B. P., and Light, B.: A Delta-Eddington multiple scattering parameterization for solar radiation
514 in the sea ice component of the Community Climate System Model, NCAR Tech. Note NCAR/TN-472+
515 STR, 1-108, 2007.

516 Bromwich, D. H., Fogt, R. L., Hodges, K. I., and Walsh, J. E.: A tropospheric assessment of the ERA -
517 40, NCEP, and JRA - 25 global reanalyses in the polar regions, *Journal of Geophysical Research:*
518 *Atmospheres*, 112, D10111, 2007.

519 Chemke, R., and Polvani, L. M.: Using multiple large ensembles to elucidate the discrepancy between
520 the 1979 - 2019 modeled and observed Antarctic sea ice trends, *Geophys. Res. Lett.*, 47, e2020G-
521 e88339G, 2020.

522 Cheng, B., Mäkynen, M., Similä, M., Rontu, L., and Vihma, T.: Modelling snow and ice thickness in the
523 coastal Kara Sea, Russian Arctic, *Ann. Glaciol.*, 54, 105-113, 2013.

524 Cheng, B., Zhang, Z., Vihma, T., Johansson, M., Bian, L., Li, Z., and Wu, H.: Model experiments on
525 snow and ice thermodynamics in the Arctic Ocean with CHINARE 2003 data, *Journal of Geophysical*
526 *Research: Oceans*, 113, C9020, 2008.

527 Collins, W. D., Bitz, C. M., Blackmon, M. L., Bonan, G. B., Bretherton, C. S., Carton, J. A., Chang, P.,
528 Doney, S. C., Hack, J. J., and Henderson, T. B.: The community climate system model version 3
529 (CCSM3), *J. Climate*, 19, 2122-2143, 2006.

530 Fairall, C. W., Bradley, E. F., Hare, J. E., Grachev, A. A., and Edson, J. B.: Bulk parameterization of air-
531 sea fluxes: Updates and verification for the COARE algorithm, *J. Climate*, 16, 571-591, 2003.

532 Fréville, H., Brun, E., Picard, G., Tatarinova, N., Arnaud, L., Lanconelli, C., Reijmer, C., and Van den
533 Broeke, M.: Using MODIS land surface temperatures and the Crocus snow model to understand the
534 warm bias of ERA-Interim reanalyses at the surface in Antarctica, *The Cryosphere*, 8, 1361-1373, 2014.

535 Frezzotti, M., Pourchet, M., Flora, O., Gandolfi, S., Gay, M., Urbini, S., Vincent, C., Becagli, S.,
536 Gagnani, R., and Proposito, M.: Spatial and temporal variability of snow accumulation in East
537 Antarctica from traverse data, *J. Glaciol.*, 51, 113-124, 2005.

538 Gascoïn, S., Lhermitte, S., Kinnard, C., Bortels, K., and Liston, G. E.: Wind effects on snow cover in
539 Pascua-Lama, Dry Andes of Chile, *Adv. Water Resour.*, 55, 25-39, 2013.

540 Granskog, M. A., Leppäranta, M., Kawamura, T., Ehn, J., and Shirasawa, K.: Seasonal development of
541 the properties and composition of landfast sea ice in the Gulf of Finland, the Baltic Sea, *Journal of*
542 *Geophysical Research: Oceans*, 109, 10.1029/2003JC001874, 2004.

543 Hao, G., Pirazzini, R., Yang, Q., Tian, Z., and Liu, C.: Spectral albedo of coastal landfast sea ice in Prydz
544 Bay, Antarctica, *J. Glaciol.*, 67, 1-11, 2020.

545 Hao, G., Yang, Q., Zhao, J., Deng, X., Yang, Y., Duan, P., Zhang, L., Li, C., and Cui, L.: Observation
546 and analysis of landfast ice arounding Zhongshan Station, Antarctic in 2016, *Haiyang Xuebao*, 9, 26-39,
547 2019.

548 Heil, P.: Atmospheric conditions and fast ice at Davis, East Antarctica: A case study, *Journal of*
549 *Geophysical Research: Oceans*, 111, C5009, 2006.

550 Heil, P., Allison, I., and Lytle, V. I.: Seasonal and interannual variations of the oceanic heat flux under a
551 landfast Antarctic sea ice cover, *Journal of Geophysical Research: Oceans*, 101, 25741-25752, 1996.

552 Hersbach, H., Bell, B., Berrisford, P., Hirahara, S., Horányi, A., Muñoz Sabater, J., Nicolas, J., Peubey,

553 C., Radu, R., and Schepers, D.: The ERA5 global reanalysis, *Q. J. Roy. Meteor. Soc.*, 146, 1999-2049,
554 2020.

555 Hersbach, H., and Dee, D.: ERA5 reanalysis is in production, *ECMWF Newsletter* 147, Reading, UK:
556 ECMWF. [Retrieved from <https://www.ecmwf.int/en/newsletter/147/news/era5-reanalysis-production>],
557 2016.

558 Hunke, E., Allard, R., Bailey, D. A., Blain, P., Craig, T., Dupont, F., DuVivier, A., Grumbine, R., Hebert,
559 D., Holland, M., Jeffery, N., Lemieux, J., Rasmussen, T., Ribergaard, M., Roberts, A., Turner, M., and
560 Winton, M.: CICE-Consortium/Icepack: Icepack1.1.1, doi:10.5281/zenodo.3251032, 2019.

561 Jakobs, C. L., Reijmer, C. H., Smeets, C. P., Trusel, L. D., Van De Berg, W. J., Van Den Broeke, M. R.,
562 and Van Wesseem, J. M.: A benchmark dataset of in situ Antarctic surface melt rates and energy balance,
563 *J. Glaciol.*, 66, 291-302, 2020.

564 Jeffries, M. O., Krouse, H. R., Hurst-Cushing, B., and Maksym, T.: Snow-ice accretion and snow-cover
565 depletion on Antarctic first-year sea-ice floes, *Ann. Glaciol.*, 33, 51-60, DOI:
566 10.3189/172756401781818266, 2001.

567 Jones, R. W., Renfrew, I. A., Orr, A., Webber, B., Holland, D. M., and Lazzara, M. A.: Evaluation of
568 four global reanalysis products using in situ observations in the Amundsen Sea Embayment, Antarctica,
569 *Journal of Geophysical Research: Atmospheres*, 121, 6240-6257, 2016.

570 Kawamura, T., Ohshima, K. I., Takizawa, T., and Ushio, S.: Physical, structural, and isotopic
571 characteristics and growth processes of fast sea ice in Lützow-Holm Bay, Antarctica, *Journal of*
572 *Geophysical Research: Oceans*, 102, 3345-3355, 10.1029/96JC03206, 1997.

573 Krumpen, T., Birrien, F., Kauker, F., Rackow, T., Albedyll, L. V., Angelopoulos, M., Belter, H. J.,
574 Bessonov, V., Damm, E., and Dethloff, K.: The MOSAiC ice floe: sediment-laden survivor from the
575 Siberian shelf, *The Cryosphere*, 14, 2173-2187, 2020.

576 Lei, R., Li, Z., Cheng, B., Zhang, Z., and Heil, P.: Annual cycle of landfast sea ice in Prydz Bay, east
577 Antarctica, *Journal of Geophysical Research: Oceans*, 115, C2006, 2010.

578 Leppäranta, M.: A growth model for black ice, snow ice and snow thickness in subarctic basins,
579 *Hydrology Research*, 14, 59-70, 1983.

580 Lindsay, R., Wensnahan, M., Schweiger, A., and Zhang, J.: Evaluation of seven different atmospheric
581 reanalysis products in the Arctic, *J. Climate*, 27, 2588-2606, 2014.

582 Lindsay, R., and Schweiger, A.: Arctic sea ice thickness loss determined using subsurface, aircraft, and
583 satellite observations, *The Cryosphere*, 9, 269-283, 2015.

584 Liston, G. E., Polashenski, C., Rösel, A., Itkin, P., King, J., Merkouriadi, I., and Haapala, J.: A distributed
585 snow - evolution model for sea - ice applications (SnowModel), *Journal of Geophysical Research:*
586 *Oceans*, 123, 3786-3810, 2018.

587 Liu, C., Gao, Z., Yang, Q., Han, B., Wang, H., Hao, G., Zhao, J., You, L., Yang, Y., Wang, L., Li, Y.:
588 Observed surface fluxes over sea ice near Antarctic Zhongshan station from April to November in 2016,
589 *Annals of Glaciology*, 61(82), 12-23, 2020.

590 Liu, C., Hao, G., Li, Y., Zhao, J., Lei, R., Cheng, B., Gao, Z., Yang, Q.: The sensitivity of
591 parameterization schemes in thermodynamic modeling of the landfast sea ice in Prydz Bay, East
592 Antarctica, *Journal of Glaciology*, 1-16, 2022.

593 Massom, R. A., Eicken, H., Hass, C., Jeffries, M. O., Drinkwater, M. R., Sturm, M., Worby, A. P., Wu,
594 X., Lytle, V. I., and Ushio, S.: Snow on Antarctic sea ice, *Rev. Geophys.*, 39, 413-445, 2001.

595 Massonnet, F., Fichet, T., Goosse, H., Vancoppenolle, M., Mathiot, P., and König Beatty, C.: On the
596 influence of model physics on simulations of Arctic and Antarctic sea ice, *The Cryosphere*, 5, 687-699,

597 2011.

598 Maykut, G. A., and Untersteiner, N.: Some results from a time-dependent thermodynamic model of sea
599 ice, *Journal of Geophysical Research (1896-1977)*, 76, 1550-1575, 10.1029/JC076i006p01550, 1971.

600 Maykut, G. A., and McPhee, M. G.: Solar heating of the Arctic mixed layer, *Journal of Geophysical*
601 *Research: Oceans*, 100, 24691-24703, 1995.

602 McPhee, M. G., Kottmeier, C., and Morison, J. H.: Ocean Heat Flux in the Central Weddell Sea during
603 Winter, *J. Phys. Oceanogr.*, 29, 1166-1179, 10.1175/1520-0485(1999)029<1166:OHFITC>2.0.CO;2,
604 1999.

605 Merkouriadi, I., Liston, G. E., Graham, R. M., and Granskog, M. A.: Quantifying the potential for snow -
606 ice formation in the Arctic Ocean, *Geophys. Res. Lett.*, 47, e2019G-e85020G, 2020.

607 Parkinson, C. L.: A 40-y record reveals gradual Antarctic sea ice increases followed by decreases at rates
608 far exceeding the rates seen in the Arctic, *Proceedings of the National Academy of Sciences*, 116, 14414-
609 14423, 2019.

610 Parkinson, C. L., and Cavalieri, D. J.: Antarctic sea ice variability and trends, 1979-2010, *The Cryosphere*,
611 6, 871-880, 2012.

612 Perovich, D. K., and Maykut, G. A.: Solar heating of a stratified ocean in the presence of a static ice
613 cover, *Journal of Geophysical Research: Oceans*, 95, 18233-18245, 10.1029/JC095iC10p18233, 1990.

614 Provost, C., Sennéchaël, N., Miguet, J., Itkin, P., Rösel, A., Koenig, Z., Villaciers Robineau, N., and
615 Granskog, M. A.: Observations of flooding and snow - ice formation in a thinner Arctic sea - ice regime
616 during the N - ICE2015 campaign: Influence of basal ice melt and storms, *Journal of Geophysical*
617 *Research: Oceans*, 122, 7115-7134, 2017.

618 Roussel, M., Lemonnier, F., Genthon, C., and Krinner, G.: Brief communication: Evaluating Antarctic
619 precipitation in ERA5 and CMIP6 against CloudSat observations, *The Cryosphere*, 14, 2715-2727, 2020.

620 Saloranta, T. M.: Modeling the evolution of snow, snow ice and ice in the Baltic Sea, *Tellus A: Dynamic*
621 *Meteorology and Oceanography*, 52, 93-108, 2000.

622 Schlosser, E., Haumann, F. A., and Raphael, M. N.: Atmospheric influences on the anomalous 2016
623 Antarctic sea ice decay, *The Cryosphere*, 12, 1103-1119, 2018.

624 Stroeve, J. C., Serreze, M. C., Holland, M. M., Kay, J. E., Malanik, J., and Barrett, A. P.: The Arctic' s
625 rapidly shrinking sea ice cover: a research synthesis, *Climatic Change*, 110, 1005-1027, 2012.

626 Stuecker, M. F., Bitz, C. M., and Armour, K. C.: Conditions leading to the unprecedented low Antarctic
627 sea ice extent during the 2016 austral spring season, *Geophys. Res. Lett.*, 44, 9008-9019, 2017.

628 Tanji, S., Inatsu, M., and Okaze, T.: Development of a snowdrift model with the lattice Boltzmann
629 method, *Progress in Earth and Planetary Science*, 8, 1-16, 2021.

630 Tetzner, D., Thomas, E., and Allen, C.: A Validation of ERA5 Reanalysis Data in the Southern Antarctic
631 Peninsula—Ellsworth Land Region, and Its Implications for Ice Core Studies, *Geosciences*, 9, 289, 2019.

632 Thiery, W., Gorodetskaya, I. V., Bintanja, R., Van Lipzig, N., Van den Broeke, M. R., Reijmer, C. H.,
633 and Kuipers Munneke, P.: Surface and snowdrift sublimation at Princess Elisabeth station, East
634 Antarctica, *The Cryosphere*, 6, 841-857, 2012.

635 Tsamados, M., Feltham, D. L., and Wilchinsky, A. V.: Impact of a new anisotropic rheology on
636 simulations of Arctic sea ice, *Journal of Geophysical Research: Oceans*, 118, 91-107, 2013.

637 Turner, A. K., Hunke, E. C., and Bitz, C. M.: Two modes of sea-ice gravity drainage: A parameterization
638 for large - scale modeling, *Journal of Geophysical Research: Oceans*, 118, 2279-2294, 2013.

639 Turner, A. K., and Hunke, E. C.: Impacts of a mushy-layer thermodynamic approach in global sea-ice
640 simulations using the CICE sea-ice model, *Journal of Geophysical Research: Oceans*, 120, 1253-1275,

641 2015.

642 Turner, J., Phillips, T., Marshall, G. J., Hosking, J. S., Pope, J. O., Bracegirdle, T. J., and Deb, P.:

643 Unprecedented springtime retreat of Antarctic sea ice in 2016, *Geophys. Res. Lett.*, 44, 6868-6875,

644 2017. Uotila, P., Goosse, H., Haines, K., Chevallier, M., Barthélemy, A., Bricaud, C., Carton, J., Fučkar,

645 N., Garric, G., and Iovino, D.: An assessment of ten ocean reanalyses in the polar regions, *Clim. Dynam.*,

646 52, 1613-1650, 2019.

647 Urraca, R., Huld, T., Gracia-Amillo, A., Martinez-de-Pison, F. J., Kaspar, F., and Sanz-Garcia, A.:

648 Evaluation of global horizontal irradiance estimates from ERA5 and COSMO-REA6 reanalyses using

649 ground and satellite-based data, *Sol. Energy*, 164, 339-354, 2018.

650 Van Den Broeke, M. R., Winther, J., Isaksson, E., Pinglot, J. F., Karlöf, L., Eiken, T., and Conrads, L.:

651 Climate variables along a traverse line in Dronning Maud Land, East Antarctica, *J. Glaciol.*, 45, 295-302,

652 1999.

653 Van Den Broeke, M. R., Reijmer, C. H., and Van De Wal, R. S.: A study of the surface mass balance in

654 Dronning Maud Land, Antarctica, using automatic weather stations, *J. Glaciol.*, 50, 565-582, 2004.

655 Van Den Broeke, M., Reijmer, C., and Van De Wal, R.: Surface radiation balance in Antarctica as

656 measured with automatic weather stations, *Journal of Geophysical Research: Atmospheres*, 109, 2004.

657 Vancoppenolle, M., Timmermann, R., Ackley, S. F., Fichefet, T., Goosse, H., Heil, P., Leonard, K. C.,

658 Lieser, J., Nicolaus, M., and Papakyriakou, T.: Assessment of radiation forcing data sets for large-scale

659 sea ice models in the Southern Ocean, *Deep Sea Research Part II: Topical Studies in Oceanography*, 58,

660 1237-1249, 2011.

661 Vignon, É., Traullé, O., and Berne, A.: On the fine vertical structure of the low troposphere over the

662 coastal margins of East Antarctica, *Atmos. Chem. Phys.*, 19, 4659-4683, 2019.

663 Wang, C., Graham, R. M., Wang, K., Gerland, S., and Granskog, M. A.: Comparison of ERA5 and ERA-

664 Interim near-surface air temperature, snowfall and precipitation over Arctic sea ice: effects on sea ice

665 thermodynamics and evolution, *The Cryosphere*, 13, 1661-1679, 2019b.

666 Wang, G., Hendon, H. H., Arblaster, J. M., Lim, E., Abhik, S., and van Rensch, P.: Compounding tropical

667 and stratospheric forcing of the record low Antarctic sea-ice in 2016, *Nat. Commun.*, 10, 1-9, 2019a.

668 Wang, Y., Zhou, D., Bunde, A., and Havlin, S.: Testing reanalysis data sets in Antarctica: Trends,

669 persistence properties, and trend significance, *Journal of Geophysical Research: Atmospheres*, 121, 12-

670 839, 2016.

671 Yang, Q., Liu, J., Leppäranta, M., Sun, Q., Li, R., Zhang, L., Jung, T., Lei, R., Zhang, Z., and Li, M.:

672 Albedo of coastal landfast sea ice in Prydz Bay, Antarctica: Observations and parameterization, *Adv.*

673 *Atmos. Sci.*, 33, 535-543, 2016a.

674 Yang, Y., Zhijun, L., Leppäranta, M., Cheng, B., Shi, L., and Lei, R.: Modelling the thickness of landfast

675 sea ice in Prydz Bay, East Antarctica, *Antarct. Sci.*, 28, 59-70, 2016b.

676 Zhang, J.: Increasing Antarctic sea ice under warming atmospheric and oceanic conditions, *J. Climate*,

677 20, 2515-2529, 2007.

678 Zhang, J.: Modeling the impact of wind intensification on Antarctic sea ice volume, *J. Climate*, 27, 202-

679 214, 2014.

680 Zhao, J., Cheng, B., Yang, Q., Vihma, T., and Zhang, L.: Observations and modelling of first-year ice

681 growth and simultaneous second-year ice ablation in the Prydz Bay, East Antarctica, *Ann. Glaciol.*, 58,

682 59-67, 2017.

683 Zhao, J., Cheng, B., Vihma, T., Yang, Q., Hui, F., Zhao, B., Hao, G., Shen, H., and Zhang, L.:

684 Observation and thermodynamic modeling of the influence of snow cover on landfast sea ice thickness

685 in Prydz Bay, East Antarctica, Cold Reg. Sci. Technol., 168, 102869, 2019.
686